This manuscript has been accepted for publication in Composite Structures

The Role of Broken Fibres on Crack Migration into 0° Surface Plies in Adhesively Bonded Carbon Fibre Composite Joints

Aakash Paul[1], Xiaodong Xu[1,2*], Takayuki Shimizu[3], Michael R. Wisnom[1]

[1] Bristol Composites Institute (ACCIS), University of Bristol, University Walk, Bristol BS8 1TR, UK

[2] University of the West of England, Coldharbour Lane, Bristol BS16 1QY, UK

[3] Research & Innovation Centre, Mitsubishi Heavy Industries, LTD. 10, Oye-cho, Minato-ku, Nagoya, 455-8515, Japan

ABSTRACT

Crack migration into the composite in adhesively bonded joints can cause a major degradation of strength. This usually occurs via cracks in the surface plies, but this paper demonstrates that crack migration can occur in joints even with 0° surface plies. The role of surface treatment is investigated by comparing grit blasted and plasma surface treatment before the secondary bonding process. Unidirectional Double Cantilever Beam specimens and quasi-isotropic Double Lap Joints with surface 0° plies were tested. It was found that with grit blasted specimens, crack migration occurred due to broken fibres present on the composite surface. Plasma treated specimens with no broken fibres on the surface failed in the adhesive with substantial increases in the Mode I fracture toughness and the strength of the double lap joints.

Keywords: Adhesive Joints; Crack Migration; Delamination; Surface Treatments

1. INTRODUCTION

Joining similar or dissimilar materials is an integral part of the design process. An adhesively bonded joint offers lower weight, enhanced fatigue life and a more uniform stress distribution when compared to the traditional mechanical fastening methods,

*Corresponding author: xiaodong.xu@uwe.ac.uk (Dr X. Xu)

therefore it is a desirable option. The use of carbon fibre composites as adherends for adhesive joints is also an attractive option for engineers due to the advanced properties of composites, such as high strength to weight ratio and improved fatigue life compared to metallic structures [1].

It is important to understand how adhesive joints fail as they are widely used in aircraft structures. The different types of failures for adhesive/composite systems and the means of accurately characterising the failure are described in the ASTM D5573 standard [2]. Cohesive failure is when the failure occurs within the adhesive. This indicates that a good adhesive bond has been obtained, and the failure is dominated by the adhesive properties. Adhesive failure is where the failure occurs at the adhesive/adherend interface. This typically means the interfacial strength is weaker than the adhesive/adherend strength, for example due to poor surface treatment. Light Fibre-Tear Failure is another type of failure which is defined in the ASTM D5573 standard. This failure occurs within the matrix of the composite adherend, i.e., interlaminar failure within the composite, close to the interface, leaving a thin layer of fibres exposed on the surface. This requires the fibres to fracture but is not clear how these strong fibres break and how the crack migrates into the composites rather than breaking the relatively weaker adhesive. Also, the strength of the matrix in carbon/epoxy composites is typically higher than the yield stress of the adhesive, again making it surprising that failure occurs in the composite.

Crack migration in composites is defined as when the delamination crack path changes from one interface to another. Krueger et al [3] showed that for an adhesively bonded flange to skin configuration using a 45° surface ply, a crack initiated in the adhesive at the flange tip and then migrated into the composite through a matrix crack in the 45° ply

during loading. This phenomenon is commonly observed in laminates e.g. [4-6], and is described by Gong et al. [7, 8] for angle-ply Double Cantilever Beam (DCB) tests. The authors stated that the crack migration occurred through the presence of ply splits, which formed due to high matrix stresses. As the off-axis plies are prone to ply splits, migration occurred until the delamination reached the 0° ply which prevented further migration. The 0° plies are expected to act as crack stoppers as the crack would need to break the 0° plies to propagate through this layer, hence why it is important to conduct characterisation tests using UD laminates. However, migration has also been observed in cases with 0° surface plies, although this would not be expected because it requires breaking fibres. For example, in adhesive joint characterisation tests, Leone et al. [9] reported a secondary delamination which developed in the 0° composite ply adjacent to the adhesive as shown in Figure 1. This was called double delamination and observed for some Mode I and low mode mixity mixed-mode tests for adhesives with composite UD adherends. Once the delamination in the 0° plies of the composite was initiated, the propagation was unstable and prevented further damage in the adhesive. The authors reported that the crack propagation within the composite caused the bridging fibres to bend and then break. However, what controlled the initial delamination was not clear. Migration was also found by Ni et al. [10], in nanostitched UD composites DCB tests. Here, the crack path moved from the ply interface into the interlaminar regions of the adjacent plies and propagated parallel to the ply interface.

Certain surface treatments can have a significant effect on the joint performance, particularly for a secondary bonding configuration, where the pre-cured adherends are bonded with adhesives. An effective surface treatment can: (i) remove weak boundary layers at the surface, such as contaminants, oxidised layers, low molecular weight

species, (ii) improve wetting of low-energy surfaces, (iii) modify the surface by the addition of polar groups or coupling agents, (iv) increase surface roughness resulting in improved mechanical interlocking and increased bonded area [11]. Sandpaper, grit blasting and peel plies are examples of surface treatment methods, where the surface roughness and area are increased [12, 13]. Plasma treatment increases the joint strength by activating the surface [14]. Other methods are also available such as laser [15], flame based treatments [16] and UV light irradiation with ozone gas [17].

Crack migration in adhesive joints has been found to be influenced by the choice of surface treatment. Encinas et al. [18] reported migration into the 0° surface ply and showed that the Mode I fracture energy (G_{IC}) for plasma treatment was higher than for the grit blasted surface treatment, but the reason for migration was not explained. The effects of untreated, sanded and plasma treatment combined with chemical treatment on the lap shear strength and G_{IC} was investigated by Jölly et al. [19] on UD composite adherends. The sanded specimens had the highest strength and toughness, and both sanded, and combined plasma and chemically treated specimens were significantly stronger and tougher than the untreated specimens. Crack migration was observed for sanded lap shear and G_{IC} tests but was not explained. Park et al. [20] reported that for UD composite single lap joints (SLJ) with epoxy adhesive under static loading, grit blasted surface preparation gives good strengths, with 0° plies visible on the fracture surfaces. This means that the crack had migrated into the surface ply, but no conclusive explanation was given to why crack migration into the surface 0° plies occurred or the role of the surface treatment.

The aim of this study is to demonstrate the effects of crack migration in the surface 0° plies of adhesively bonded carbon fibre composite joints and to understand why this

occurs. Two different surface treatments were used to avoid undesirable adhesive failure. A grit blasted surface treatment, which offers a good bond but introduces broken fibres on the surface at the microscopic scale, and plasma treatment, which results in a good bond without broken fibres.

G_{IC} was measured from DCB tests for two nominal adhesive thicknesses of 0.2 mm and 0.8 mm which are typical adhesive thicknesses used by industry. Double Lap Joint (DLJ) tests were also conducted with both grit blasted and plasma surface treatments to demonstrate the implications of crack migration for structural applications.

2. EXPERIMENTAL SETUP

2.1 Manufacturing Configurations

The material for the composite adherends used was Hexcel's HexPly® IM7/8552 carbon/epoxy prepreg with a nominal thickness of 0.125 mm. The adhesive used was Hexcel's Redux 319® 367 g/m^2 unsupported film adhesive with a nominal cured thickness of 0.2 mm and no carrier.

2.1.1 Double Cantilever Beam Manufacturing

The manufacturing for the characterisation test specimens is explained in this section. The layup of the unidirectional IM7/8552 laminates was done first with a stacking sequence of $[0]_{20}$. The curing cycle for the laminates was in two stages. The autoclave was heated up to 125˚C at a ramp-up rate of 2˚C/min and held at this temperature for 100 minutes, followed by a ramp to 185˚C at 2˚C/min and held for 165 minutes. The pressure was increased at 69 kPa per minute to 690 kPa, which was kept throughout the cycle under vacuum. The adhesive was bonded using a secondary bonding technique. Two batches were created using the two surface preparation techniques, which are

described in Section 2.2. Following the surface preparation, the composite adherends were bonded with the adhesive over the entire treated surface to maintain a consistent bondline thickness. A layer of release film was inserted between the adhesive and adherend for the 0.2 mm nominal adhesive thickness case and between the middle adhesive layers for the 0.8 mm nominal adhesive thickness case. This results in slight asymmetry with the starter film on one side of the 0.2 mm nominal adhesive thickness, but it should not affect the results. Crack migration occurred very quickly with or without a symmetrical geometry as shown later in the 0.8 mm nominal adhesive thickness case where the film was in the centre of the adhesive layer. The material used for the insert was the Flomfilm 100 cast PTFE film, with a thickness of 12 μm. The adhesive was cured at 175˚C for 1 hour at 690 kPa. The ramp-up rate specified in the data sheet was 5˚C/min. Hinges for the DCB tests were bonded using Huntsman's Araldite® 2014-1 paste adhesive. The curing cycle used for the paste adhesive was 80˚C for 1 hour with use of gentle clamping at standard atmospheric pressure.

2.1.2 Double Lap Joints Manufacturing

The schematic for the typical DLJ specimen is shown in Figure 2a. The layup of the IM7/8552 laminates was done first, following the same curing cycle as defined in Section 2.1.1. The stacking sequence of the adherends was quasi-isotropic (QI), $[0/45/90/-45]_{2s}$. The adhesive thickness is 0.2 mm. Adhesive fillets were not deliberately introduced but were formed during manufacturing and the precise geometry was variable. After the surface treatment of the QI laminates, they were bonded with the film adhesive in the configuration shown in Figure 3. The schematic shows two half joints bonded with the film adhesive. Spacers made of the same material were used to ensure constant adhesive thickness was achieved throughout the joint and minimum leakage of

adhesive during the curing process, and to allow flat tooling. The cured spacers were then bonded with a layer of adhesive and separated by the release film, which is highlighted in red in Figure 3. The release film ensured that after the curing process, the spacers could be separated from the adherends. The Redux 319 film adhesive was cured at 175˚C for 1 hour at 690 kPa. The ramp-up rate specified in the data sheet of 5˚C/min was used. Gaps can arise due to dimensional tolerances in the composite cutting process. During the curing process, the adhesive can flow away from the bondline if there are gaps between the laminates and spacers as highlighted in Figure 3. The fillet formation was not controlled for the DLJ cases and the fillet shapes were variable. After the secondary bonding process was completed, paste adhesive (Huntsman's Araldite® 2014-1) was used to bond the two half joints obtained and form a symmetrical DLJ with a 4 mm thick inner adherend at the mid-plane as shown in Figure 2a. The curing cycle used for the paste adhesive was 80˚C for 1 hour with use of gentle clamping at the standard atmospheric pressure.

2.2 Surface Treatment

This section introduces the two surface treatments, grit blasting and plasma treatment, used in this study for the DCB and DLJ tests. Both treatments were applied after manufacturing the composite adherends and before the secondary bonding procedure.

2.2.1 Grit Blasting

A Vacu-Blast International (Wheelabrator)'s shot blaster was used to obtain a macroscopically rough surface. The specimens were carefully inspected to make sure there was a similar degree of glossiness on the surface corresponding to the removal of surface resin and exposure of the fibres. The available grit size of 165 μm and blast standard pressure of 4 bars were used. Care was taken to ensure no debris was left after

grit blasting by applying concentrated high-pressure air and cleaning with a micro-fibre towel, as debris can have a critical effect on the bond strength. Liquid degreasing with acetone was subsequently used to remove oils and other potential organic contaminants from the surfaces immediately prior to bonding.

Figure 4 shows the Scanning Electron Microscope (SEM) images for the grit blasted specimen surfaces. Multiple discontinuous fibres were observed, damaged during the grit blasting process. Hence, broken fibres were present on the adherend surface before the secondary bonding process when the specimens were grit blasted.

2.2.2 Plasma Treatment

Plasma treatments work by altering the surface of a polymer by attaching polar or functional groups to it. The UV radiation and active oxygen species from the plasma break up separating agents, silicones and oils from the composite surface. The active oxygen species (radicals) from the plasma bind to active surface sites all over the material, creating a surface that is highly ‘active’ to bonding agents.

Diener Electronic’s Femto, a low-pressure plasma system, was used for the plasma treatment. The samples were placed 75 mm from the chamber gas discharge nozzle and exposed to the plasma for 1 minute. The power was set at 100 W and the gas composition was 100% oxygen, i.e. no secondary gas. No visible change in the surface texture was observed and no broken fibres were observed after plasma treatment. A clear difference in the contact angle was observed in water droplet tests comparing untreated and plasma treated samples. The specimen without the plasma treatment had water droplets with an elliptical shape whereas the plasma treated specimen water droplets were almost flat on the surface, which indicates successful surface preparation.

Following the plasma treatment, the specimens were bonded in the autoclave after approximately 3 hours.

2.3 Specimen Configurations

2.3.1 Double Cantilever Beam Tests

The DCB tests were conducted in accordance with the ASTM D5528 standard for the Mode I interlaminar fracture toughness of unidirectional carbon fibre composites. The G_{IC} values were calculated according to the Modified Beam Theory (MBT) as recommended in previous research [21]. Figure 2b shows the schematic for the DCB specimen according to the ASTM D5528 standard, where *b*, the specimen width, was 20 mm, *L*, the specimen length, was 140 mm, *h*, the specimen thickness was 2.5 mm. The 0.2 mm adhesive thickness grit blasted specimens had an a_0 of approximately 50 mm, whereas all other cases had an a_0 of approximately 55 mm. The variation is acceptable as per the ASTM D5528 standard. It only affects the stiffness in the force-displacement curves obtained and the a_0 is taken into account in the G_{IC} calculation.

These dimensions were held constant for all the DCB tests. The nominal adhesive thicknesses were used and were similar to the actual measured adhesive thickness. The loading rate during the DCB testing was 2 mm/min. A Shimadzu screw-driven universal machine was used to conduct the DCB tests. The ASTM D5528 standard states that if the response is nonlinear, it is recommended to use the G_{IC} calculated from the load 5% offset from the initial linear response (P5%). This P5% value was therefore used as it represents the lower bound value for the G_{IC} for cases where significant non-linearity is present. For cases with no or limited non-linearity before the load drop, the maximum load was used. At least 3 specimens were tested for each configuration. Figure 5a shows the schematic for the 0.2 mm nominal adhesive thickness (1 layer of film adhesive)

DCB specimen. The PTFE film (highlighted in orange in Figure 5a) was placed at the adherend/adhesive interface as shown in Figure 5a. Figure 5b shows the schematic for the 0.8 mm nominal adhesive thickness (4 layer of film adhesive) DCB specimen. The PTFE film was placed between the centre two layers of adhesive, at the mid-plane, as shown in Figure 5b.

2.3.2 Double Lap Joints Tests

Figure 2a showed the DLJ specimen configuration and dimensions. The tests were conducted using an Instron hydraulic-driven test machine. Tensile testing of the double lap joints was conducted under displacement control at a loading rate of 0.5 mm/min and 4 specimens were tested for each configuration. The DLJ strength was based on the maximum load before catastrophic failure.

3. DOUBLE CANTALEVER BEAM (DCB) RESULTS AND DISCUSSION

3.1 0.2 mm Nominal Adhesive Thickness

3.1.1 Grit Blasted

It was observed that during the tests, the crack propagation was sudden, unstable and catastrophic, as shown in the force-displacement curve for a typical grit blasted specimen in Figure 6. As nonlinearity was not present, the maximum load (Pmax) was used to calculate $G_{IC.}$ During this unstable failure, the crack migrated from the adhesive/adherend interface into the surface 0° layer of the composite. The crack propagated roughly 10 mm in the composite. The G_{IC} value for the grit blasted specimen was 0.347 N/mm, as given in Table 1. As the crack propagated into the composite during the initial loading, the initial loading G_{IC} values are reported throughout this paper for consistency.

The typical fracture surface and schematic is shown in Figure 7. The composite 0° plies were visible on both fracture surfaces, showing that the crack had propagated into the adherend. It is believed that this occurred via the microscopic regions of broken fibres that were present, as can be seen in Figure 4. This suggests that the adherend properties mainly controlled the failure for the grit blasted case, and the value of G_{IC} is not that much higher than typical G_{IC} values reported for IM7/8552 (0.21 N/mm [22], 0.28 N/mm [23]).

3.1.2 Plasma Treated

During loading, a significant region of non-linearity was observed before final failure, as shown in Figure 6 for a typical specimen, hence the load 5% offset from the initial linear response (P5%) was used to calculate G_{IC}. During the non-linearity, the crack propagated from the adhesive/adherend interface into the adhesive and not into the composite. The plasma treatment initiation G_{IC} result is 0.864 N/mm, more than double the grit blasted value, as seen in Table 1. A typical fracture surface and schematic is shown in Figure 8. A cohesive failure can be observed, as the adhesive was visible on both fracture surfaces. Hence, the adhesive properties controlled the failure for the plasma treated case. Surface 0° plies at the edges of the specimen are also visible in Figure 8b. The composite surface texture before migration was the plasma treated surface, whereas this texture changes after migration into the surface 0° ply.

3.2 0.8 mm Nominal Adhesive Thickness

3.2.1 Grit Blasted

During loading, a change in stiffness before unstable crack propagation was observed, as shown in the typical load-displacement curve in Figure 10, hence the P5% load was used to calculate G_{IC}. The failure was catastrophic, represented by the sharp load drop in

Figure 10. The experimental results for the 0.8 mm nominal adhesive thickness grit blasted case are summarised in Table 1.

Figure 11 shows the typical fracture schematic and surface for the 0.8 mm case. As the insert film was placed in between the adhesive, an initial cohesive failure was observed, and a high G_{IC} suggests that the failure was controlled by the adhesive. During further loading however, the crack propagated in an asymmetric pattern, with migration into the composite occurring sooner on one side of the specimen and then propagating through the width.

3.2.2 Plasma Treated

Like the grit blasted 0.8 mm adhesive thickness the P5% load was used to calculate the G_{IC} as non-linearity was present during loading as seen in Figure 10. During curing of some 0.8 mm adhesive thickness specimens, wrinkles in the PTFE film were present as shown in Figure 12. These were formed due to movement of the insert film placed in between the adhesive layers as a result of the low adhesive viscosity at higher temperatures. These wrinkles were not believed to be critical as they were away from the crack tip. Table 2 summarises the plasma treated G_{IC} results for the 0.8 mm nominal adhesive thickness.

The fracture surfaces and schematic are shown in Figure 12 for the plasma treated 0.8 mm nominal adhesive thickness case. Analysing the fracture surface, an initial cohesive failure was observed followed by migration into the adherends from the edges. Hence, the G_{IC} for this case was also controlled by the adhesive properties.

3.3 Discussion

Analysing the force-displacement curves for both cases for the 0.2 mm nominal adhesive thickness case in Figure 6 shows a significant increase in maximum load. A discrepancy in the stiffness was observed due to the difference in a_0 length before the DCB test for the two batches as discussed in Section 2.3.1. Comparing the G_{IC} and fracture surfaces for the different surface treatments for the 0.2 mm nominal adhesive thickness cases shows a large increase of 149% in G_{IC} and a clear change in failure mode. As discussed in Section 2.2.1, the grit blasting surface treatment creates microscopic regions of broken fibres. These broken fibres can potentially introduce local high stress concentrations which could create a path for crack migration into the adherend surface 0° ply before the adhesive could yield and allow propagation in the adhesive. A sudden load drop was seen on the force-displacement curve (Figure 10) for the grit blasted tests as the crack migrated into the less tough composite before any non-linear adhesive behaviour could occur, as shown in Figure 6. The crack stayed within the adherend during propagation. For the plasma treated cases, a cohesive failure was observed. As no fibres were broken on the adherend surface during the surface preparation stage, the failure initiated from the adhesive/adherend interface into the adhesive as this was the weakest path. The failure was now controlled by the higher adhesive G_{IC} properties, giving a much higher G_{IC} than for the grit blasted surface for the 0.2 mm nominal adhesive thickness case. During propagation, it can be seen on the fracture surface in Figure 8b that some crack migration still occurred, initiating from the specimen edges. Although no broken fibres were present on the plasma treated surfaces, they do occur at the edges where the specimens were cut since the fibres are not perfectly parallel. The appearance of the fracture surface suggests that these broken

fibres at the specimen edges initiated migration of the crack into the adherend locally, but failure was still controlled primarily by the adhesive.

Analysing the G_{IC} and fracture surfaces for the 0.8 mm nominal adhesive thickness shows that the initial failure in both cases was controlled by the adhesive properties. Although the plasma treated specimen had a slightly higher G_{IC} than the grit blasted case, the difference in G_{IC} was significantly less than the 0.2 mm case, as the failure modes for the 0.8 mm cases were similar. The failure of the grit blasted specimens was unstable, i.e. a catastrophic failure at the load drop. The crack propagated within the adhesive initially and then migrated into the 0° ply in the adherend surface during the load drop. The final crack propagation path was into the adherend 0° ply, through the broken fibres on the composite surface. The failure process for the plasma treated specimens was slightly different. The failure initiated within the adhesive during the non-linear response when the adhesive yielded, consistent with the grit blasted case. However, a secondary delamination initiated in the adherend, very close to the interface during the propagation stage. Analysing the fracture surface post failure, there are 0° fibres at the edges of the specimen where the secondary delamination initiated, showing that migration had occurred into the surface 0° ply. The failure sequence is shown in Figure 13, just before and after the secondary delamination, initiating away from the adhesive. The first load drop for the plasma treated case, seen in Figure 10 represented the initiation of this secondary delamination. As the displacement increased, the two delamination paths coalesced. Observing the fracture surface, past the insert film, broken fibres were only visible on the specimen edges initially, while the adhesive was visible at the centre. This suggests that the secondary delamination that occurred within the adherend (crack into the 0° surface ply) initiated from the free edges of the adherend

where there are broken fibres and propagated progressively across the width. This was similar to the plasma treated 0.2 mm adhesive thickness case, where crack migration initiated from the specimen free edges. Although crack migration occurred for both the grit blasted and plasma treated specimens, it did not have a large effect on the G_{IC} as it only occurred after the load drop. The failure in both cases was controlled by the adhesive properties.

Increasing the adhesive thickness increases the G_{IC} for both surface preparation methods as shown in Figure 9. A greater increase was found comparing the grit blasted case to the plasma treatment case, due to the change in failure mode for the grit blasted case. The 0.2 mm nominal adhesive thickness case was controlled by the adherend properties, whereas the 0.8 mm case was controlled by the adhesive properties. For the plasma treated specimens, the failure for both 0.2 and 0.8 mm cases were cohesive, i.e. controlled by the adhesive properties. The increase in G_{IC} with adhesive thickness may be attributed to the increased energy dissipation in the process zone through increased plastic straining [24].

4. DOUBLE LAP JOINTS (DLJ) RESULTS AND DISCUSSION

Following the DCB tests, DLJ tests were conducted to understand whether the surface preparation and crack migration have a similar significant effect on the DLJ strength as observed for the 0.2 mm nominal adhesive thickness DCB case.

4.1 Grit Blasted Double Lap Joints

The force-displacement curves for all DLJ specimens were linear with a load drop at the maximum load, and failure was sudden and catastrophic. The results for the grit blasted DLJ strength are summarised in Table 2. The fracture surface and schematic are shown

in Figure 14, where the dotted line in the schematic represents the primary crack propagation path during failure. The grit blasted fracture surfaces show the surface 0° plies across all inner adherend/outer adherend interfaces, indicating that the crack had migrated into the surface ply.

The shape of the adhesive fillets for this case were not controlled during the manufacturing process. The fracture surfaces shown in Figure 14 are post failure of the whole bondline. The primary failure mechanism is explained based on images obtained from a Photron high-speed camera as shown in Figure 15. The high-speed camera video was taken at 80,000 frames per second. The high-speed camera images do not show any indication of crack initiation during the initial stages of loading. Analysing the frame before catastrophic failure, cracks were visible within the adhesive fillet and on the surface 0° ply of the inner adherend. It was not clear whether the crack initiated within the adhesive or composite first, as cracks appeared in both materials simultaneously. As the failure was sudden and catastrophic and the high-speed camera did not pick up the full failure sequence, it was postulated that the adhesive fillet yielded due to the high shear and peel components at the leading edges of the DLJ. This plastic region grew during loading and spread to the bondline resulting in crack migration into the surface 0° ply in the inner adherend as shown in Figure 15 (very close to the interface). As discussed in Section 2.2.1, the grit blasted surface treatment created broken fibres at the microscopic level, facilitating crack migration into the surface 0° ply, as seen in the DCB tests. Broken fibres were also visible on the fracture surfaces of the DLJs, as shown in Figure 16.

4.2 Plasma Treated Double Lap Joints

Similar to the grit blasted DLJ, the failure was sudden and catastrophic for the plasma treated cases. The results for the plasma treatment cases are shown in Table 2, and fracture surface images and schematic in Figure 17. The fracture surface shows the post failure surface of the whole bondline and does not indicate the sequence of the failure. The failure schematic shows the primary failure mechanism within the adhesive. For this case, patches of adhesive and 0° fibres were visible on both the fracture surfaces (highlighted in Figure 17), which suggests that the adhesive in the bondline controlled the failure for this case.

4.3 Discussion

A 78% increase in DLJ strength for the plasma treated specimens was observed compared to the grit blasted specimens, as shown in Figure 18. Comparing the failure mechanisms shows that the grit blasted case was controlled by the adherend properties as there were broken fibres present from the surface preparation stage facilitating crack migration into the adherend at failure. For the plasma treatment, patches of adhesive were visible on the fracture surface, which indicates that the adhesive had a significant influence on the failure. The 0° fibres visible on the fracture surface are believed to be a post failure effect, i.e. after the failure within the adhesive. The change in failure mechanism explains the significantly higher strength observed for the plasma treatment case compared to the grit blasted case. The failure is mixed mode, nevertheless it is interesting to note that the 78% increase in failure load is of similar order to the DCB tests, where the 149% increase in G_{IC} is consistent with a 58% increase in load since energy release rate is proportional to load squared.

The failure modes were consistent for the DCB and DLJ tests, with the grit blasted specimens controlled by the adherend properties and the plasma treated specimens controlled by the adhesive properties. These results clearly show that using a plasma treatment as surface preparation instead of grit blasting results in a cohesive failure, i.e. consistently controlled by the adhesive properties. This gives better performance for such joints as the crack migration effects are secondary.

5. CONCLUSION

Crack migration into surface 0° plies can occur due to broken fibres on the adherend surface and has a significant effect on the G_{IC} and DLJ strength for adhesive/composite systems. For the grit blasted surface preparation, microscopic regions of broken fibres were induced during the grit blasting process and facilitated crack migration into the composite. The plasma surface treatment activated the adherend surface before secondary bonding and no mechanical change in the adherend surface was observed. This produced strong joints without crack migration.

For the 0.2 mm nominal adhesive thickness, an increase of 149% in G_{IC} was observed for the plasma treated specimens compared to the grit blasted case. During the DCB test, with the PTFE film placed at the adhesive/adherend interface, the crack migrated from the adhesive/adherend interface into the adherend for the grit blasted case. The broken fibres on the adherend surface facilitated crack migration and resulted in the failure being controlled by the adherend properties. For the plasma treated case, as no broken fibres were present on the adherend surface and a good bond quality was achieved, the crack propagated into the adhesive from the adhesive/adherend interface. The failure was hence controlled by the adhesive properties. Some migration still occurred from the edge of the specimen believed to be due to cut fibres that arise during

machining since they are not perfectly parallel. As the adhesive is much tougher than the composite, a significant increase in G_{IC} was observed from the grit blasted to the plasma treated case. When the PTFE film was placed in between the adhesive layers (0.8 mm nominal adhesive thickness case), the G_{IC} values were 16% higher for the plasma treated case compared to the grit blasted case, not as large a difference as for the 0.2 mm nominal thickness case since there was no change in failure mode. For both surface treatments for the 0.8 mm case, the initial crack propagation occurred within the adhesive, and hence the failure was controlled by the adhesive. The G_{IC} for both surface treatments were higher than for the 0.2 mm nominal adhesive thickness.

Applying these surface preparation techniques to a DLJ test shows crack migration has a similarly significant effect on the DLJ strength. An increase of 78% in DLJ strength was observed for the plasma treated DLJ compared to the grit blasted DLJ. The failure mode for the grit blasted case was postulated to be failure initiating at the adhesive fillet followed by migration into the surface 0° ply of the adherend, hence was controlled by both the adhesive and composite. For the plasma treated specimen, the failure was controlled by the adhesive. The change in failure mode due to crack migration explains the difference in DLJ strength observed.

DATA AVAILABILITY

The data required to support the conclusions are provided in the results sections of this paper.

REFERENCES

[1] Adams RD, Comyn J, Wake WC. Structural adhesive joints in engineering. London: Chapman & Hall, 1997.

[2] ASTM D5573 - 99, Standard Practice for Classifying Failure Modes in Fiber-Reinforced-Plastic (FRP) Joints. ASTM; 2019.

[3] Krueger R, Cvitkovich M, O'Brien T, Minguet P. Testing and analysis of composite skin/stringer debonding under multi-axial loading. Journal of Composite Materials. 2000;34:1263-300.

[4] Ratcliffe JG, Czabaj MW, O'Brien TK. A Test for Characterizing Delamination Migration in Carbon/Epoxy Tape Laminates Hampton, Virginia National Institute of Aerospace & Langley Research Center; 2013.

[5] Canturri C, Greenhalgh ES, Pinho ST, Ankersen J. Delamination growth directionality and the subsequent migration processes – The key to damage tolerant design. Composites Part A: Applied Science and Manufacturing. 2013;54:79-87.

[6] Carvalho NVD, Chen BY, Pinho ST, Ratcliffe JG, Baiz PM, Tay TE. Modeling delamination migration in cross-ply tape laminates. Composites Part A: Applied Science and Manufacturing. 2015;71:192-203.

[7] Gong Y, Zhang B, Mukhopadhyay S, Hallett SR. Experimental study on delamination migration in multidirectional laminates under mode II static and fatigue loading, with comparison to mode I,. Composite Structures. 2018;201:683-98.

[8] Gong Y, Zhang B, Hallett SR. Delamination migration in multidirectional composite laminates under mode I quasi-static and fatigue loading. Composite Structures. 2018;189:160-76.

[9] Leone J, Frank A., Girolamo D, Dάvila CG. Progressive Damage Analysis of Bonded Composite Joints. Langley Research Center, Hampton, Virginia 23681-2199: National Aeronautics and Space Administration; 2012.

[10] Ni X, Furtado C, Fritz NK, Kopp R, Camanho PP, Wardle BL. Interlaminar to intralaminar mode I and II crack bifurcation due to aligned carbon nanotube reinforcement of aerospace-grade advanced composites. Composites Science and Technology. 2020;190.

[11] Wingfield JRJ. Treatment of composite surfaces for adhesive bonding. International Journal of Adhesion and Adhesives. 1993;13:151-6.

[12] Campbell FC. Manufacturing technology for aerospace structural materials. Elsevier; 2011.

[13] Klapprott D, Li H, Wong R, Geisendorfer G. Key factors of the peel ply surface preparation process. Henkel Corporation; 2014.

[14] Dighton C, Rezai A, Ogin SL, Watts JF. Atmospheric plasma treatment of CFRP composites to enhance structural bonding investigated using surface analytical techniques. International Journal of Adhesion and Adhesives. 2019;91:142-9.

[15] Li S, Sun T, Liu C, Yang W, Tang Q. A study of laser surface treatment in bonded repair of composite aircraft structures. Royal Society Open Science. 2018;5.

[16] Tadeka T, Yasuoka T, Hoshi H, Sugimoto S, Iwahori Y. Effectiveness of flame-based surface treatment for adhesive bonding of carbon fiber reinforced epoxy matrix composites. Composites Part A: Applied Science and Manufacturing. 2019;119:30-7.

[17] Kupski J, Teixeira de Freitas S, Zarouchas D, Camanho PP, Benedictus R. Composite layup effect on the failure mechanism of single lap bonded joints. Composite Structures. 2019;217:14-26.

[18] Encinas N, Oakley BR, Belcher MA, Blohowiak KY, Dillingham RG, Abenojar J, et al. Surface modification of aircraft used composites for adhesive bonding. International Journal of Adhesion and Adhesives. 2014;50:157-63.

[19] Jölly I, Schlögl S, Wolfahrt M, Pinter G, Fleischmann M, Kern W. Chemical functionalization of composite surfaces for improved structural bonded repairs. Composites Part B: Engineering. 2015;69:296-303.

[20] Park S-M, Roy R, Kweon J-H, Nam Y. Strength and failure modes of surface treated CFRP secondary bonded single-lap joints in static and fatigue tensile loading regimes. Composites Part A: Applied Science and Manufacturing. 2020;134:105897.

[21] Renart J, Costa J, Sarrado C, Budhe S, Turon A, Rodríguez-Bellido, A. Mode I fatigue behaviour and fracture of adhesively-bonded fibre-reinforced polymer (FRP) composite joints for structural repairs. Fatigue and Fracture of Adhesively-Bonded Composite Joints: University of Girona, Girona, Spain, AIRBUS Operations, Madrid, Spain; 2015.

[22] Hansen P, Martin RH. DCB, 4ENF and MMB Delamination Characterisation of S2/8552 and IM7/8552. London, England: European Research Office of the US Army; 1999.

[23] Camanho PP, Lambert M. A Design Methodology for Mechanically Fastened Joints in Laminated Composite Materials. Composites Science and Technology. 2006;66:3001-20.

[24] Belnoue JP-H, Hallett SR. Cohesive/adhesive failure interaction in ductile adhesive joints Part I: A smeared-crack model for cohesive failure. International Journal of Adhesion and Adhesives. 2016;68:359-68.

Figures and Tables

Figure 1 - Example of double delamination [9].

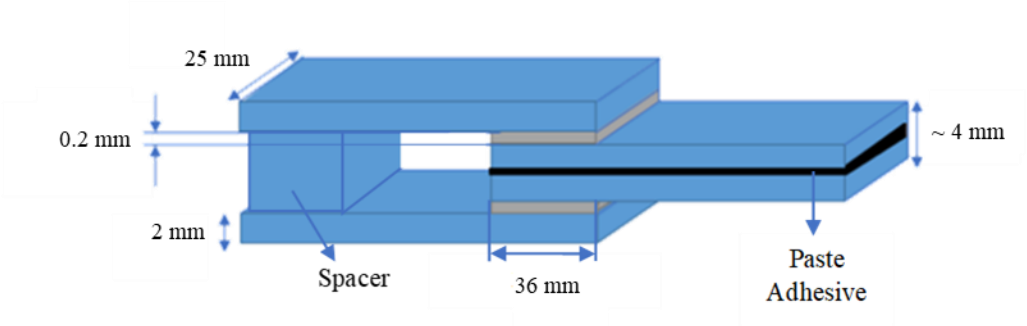

a) Schematic of the double lap joint

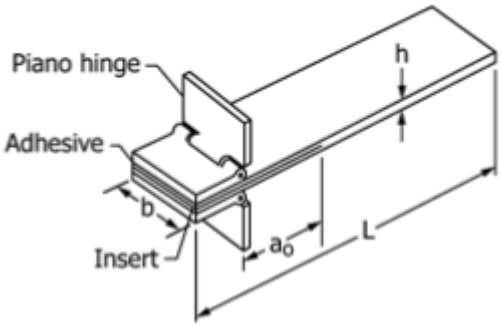

b) Schematic of DCB according to ASTM D5528 [2]

Figure 2 – Schematics of the typical specimen for the DLJ and DCB tests.

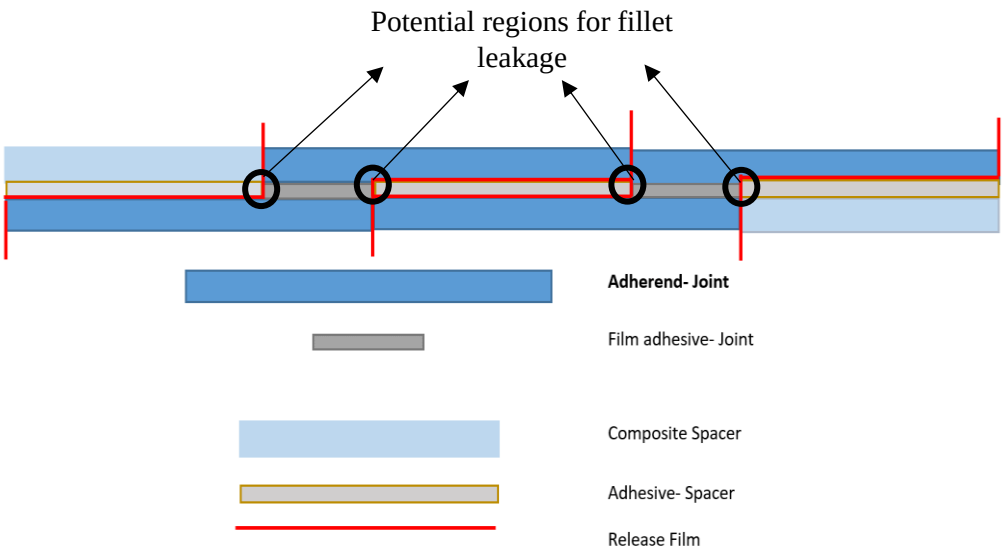

Figure 3 - Schematic of the initial bonding configuration for the two half joints.

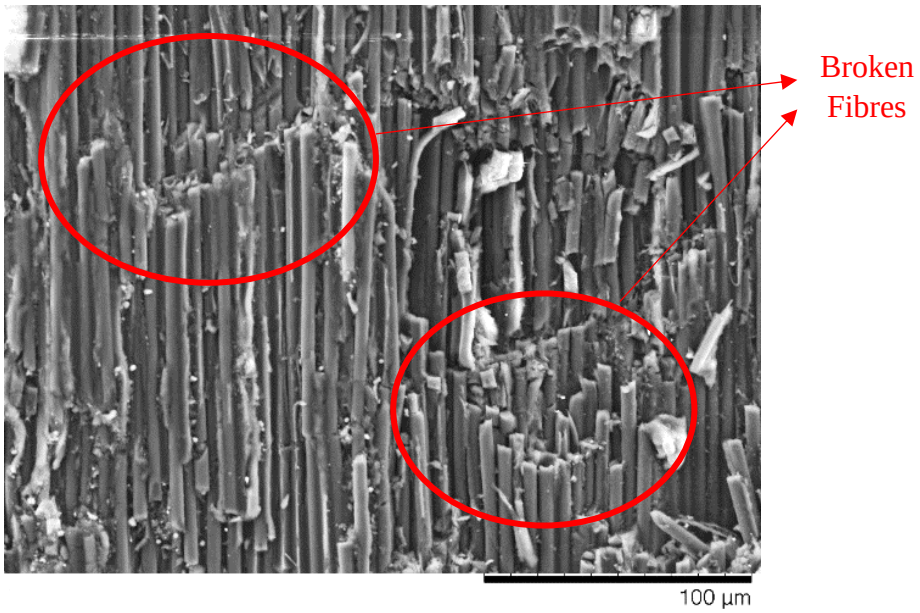

Figure 4 - SEM image of the grit blasted surface of a DCB specimen before secondary bonding.

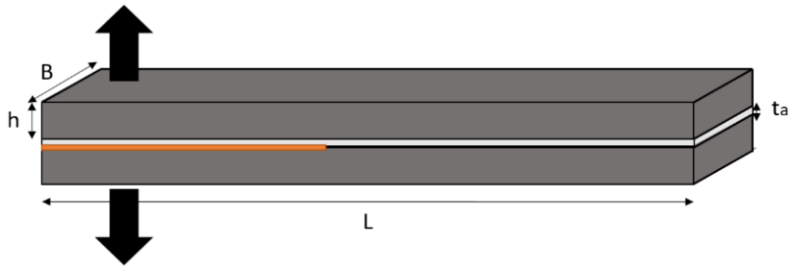

a) 0.2 mm nominal adhesive thickness DCB specimen

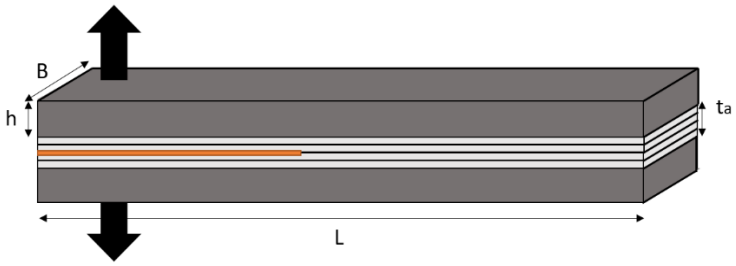

b) 0.8 mm nominal adhesive thickness DCB specimen

Figure 5 - Schematic of the DCB specimens used for testing.

Figure 6 - Typical load displacement curves for the 0.2 mm nominal adhesive thickness DCB cases.

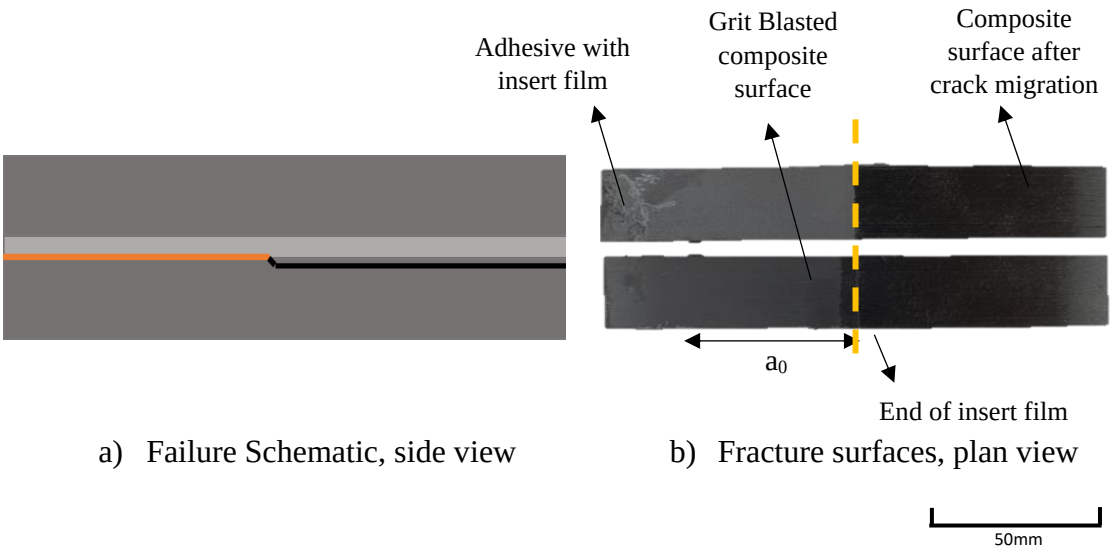

a) Failure Schematic, side view b) Fracture surfaces, plan view

Figure 7 - Failure schematic and fracture surfaces for the grit blasted 0.2mm DCB specimens.

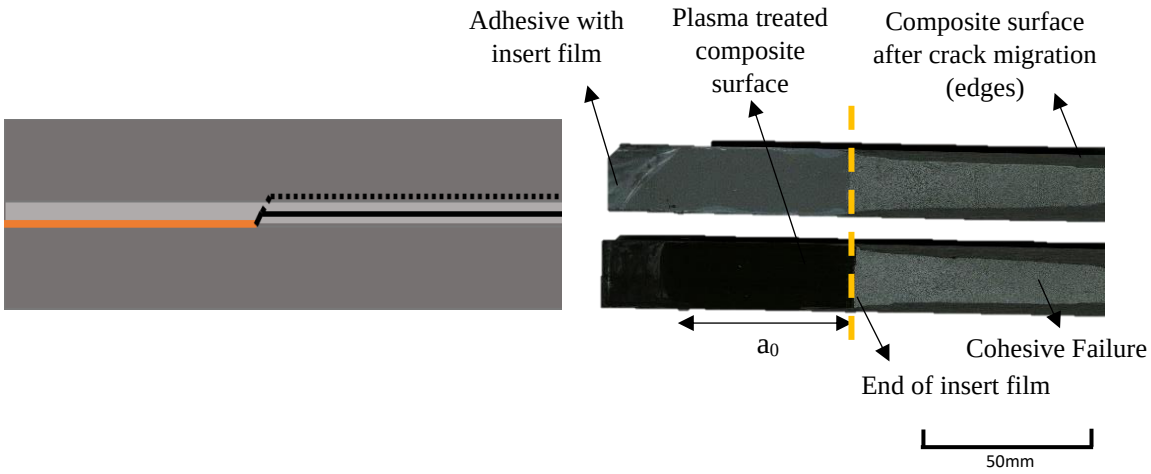

a) Failure Schematic, side view b) Fracture surfaces, plan view

Figure 8 - Failure schematic and fracture surfaces for the plasma treated 0.2 mm DCB specimens where the solid lines represent the primary failure mechanism and dotted lines represent the secondary failure mechanism at the edges.

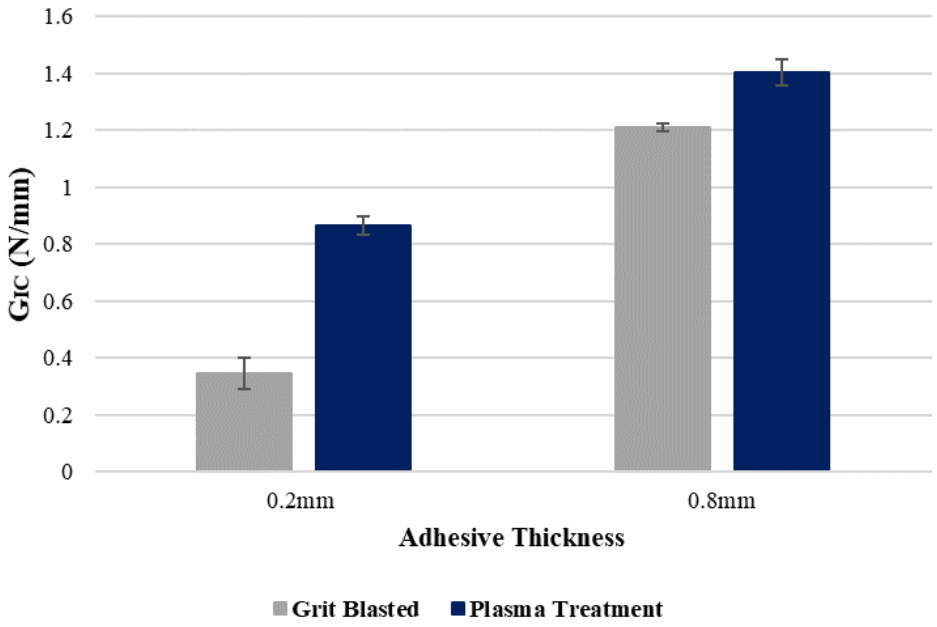

Figure 9 - Comparison of grit blasted and plasma treated G_{IC}.

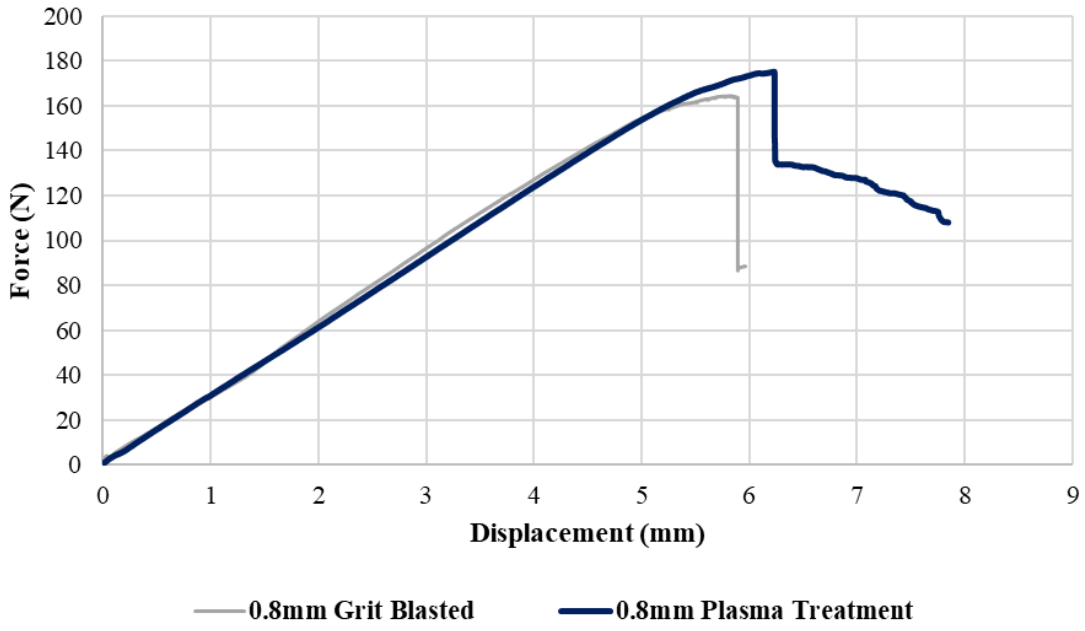

Figure 10 - Typical load displacement curves for the 0.8 mm nominal adhesive thickness DCB cases.

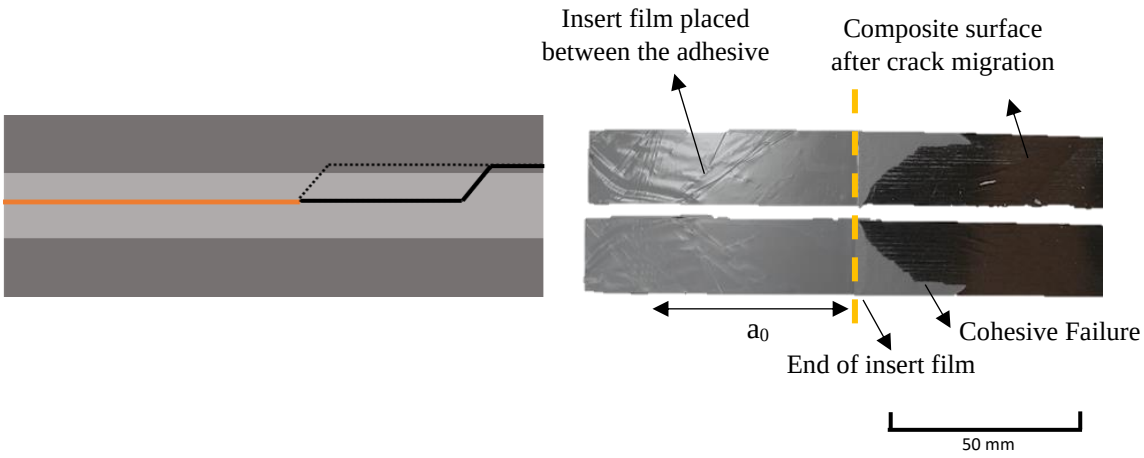

a) Failure Schematic, side view b) Fracture surfaces, plan view

Figure 11 - Typical failure schematic and fracture surfaces for 0.8 mm nominal adhesive thickness DCB tests using grit blasted surface treatment where the solid lines represent the primary failure mechanism and dotted lines represent the secondary failure mechanism at one edge.

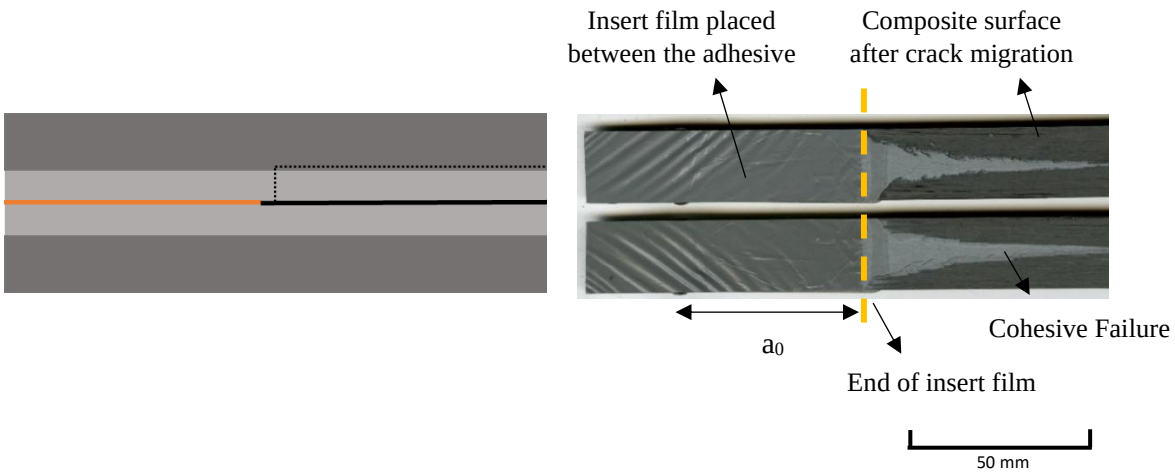

a) Failure Schematic, side view b) Fracture surfaces, plan view

Figure 12 - Typical failure schematic and fracture surfaces for 0.8 mm nominal adhesive thickness DCB tests using plasma surface treatment where the solid lines represent the primary failure mechanism and dotted lines represent the secondary failure mechanism at the edges.

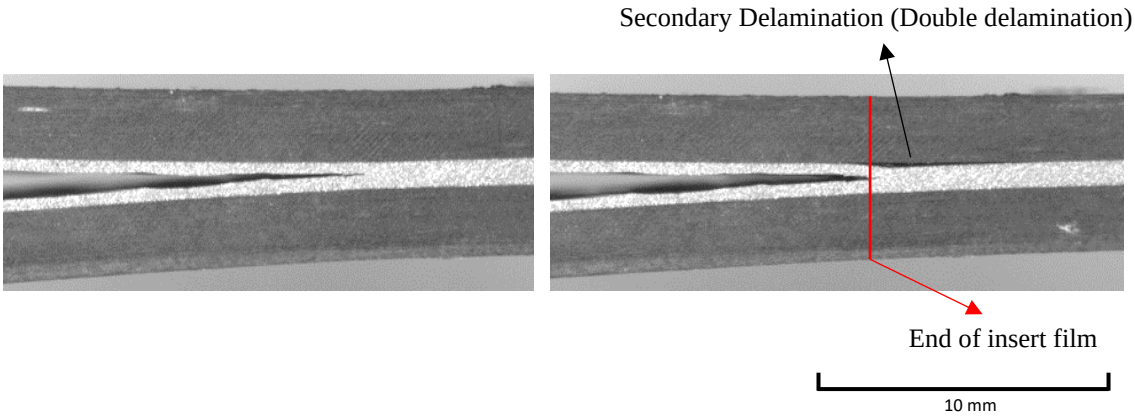

Figure 13 - Failure sequence capturing the double delamination for the 0.8 mm adhesive thickness plasma treated specimen.

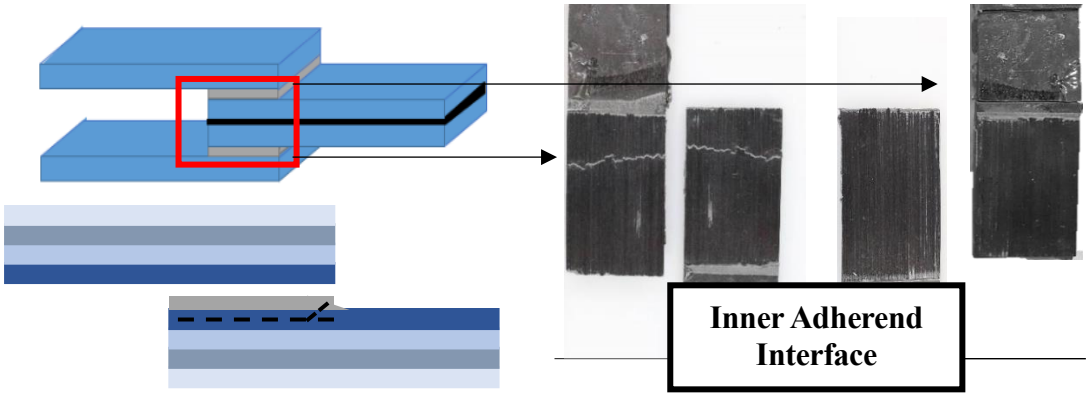

a) Schematic b) Fracture surface

Figure 14 - Failure schematic and fracture surface for grit blasted DLJ specimen.

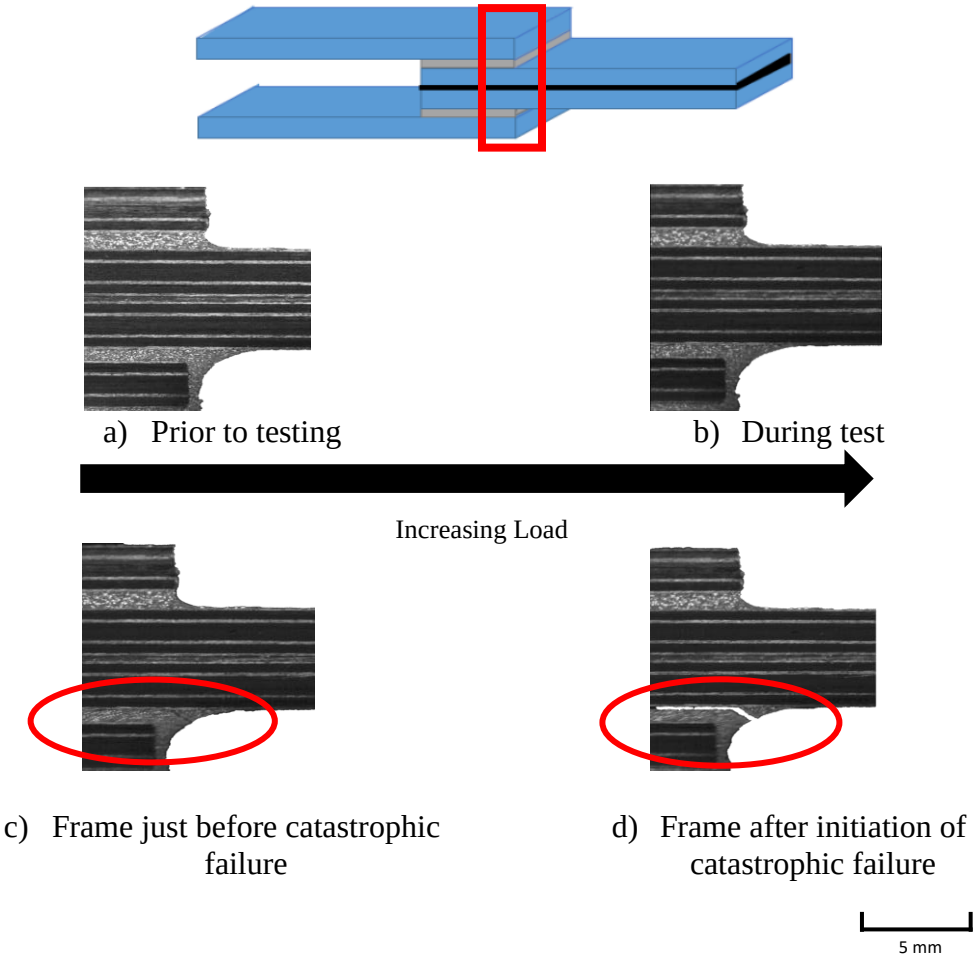

Figure 15 - High-speed camera images for grit blasted DLJ specimen.

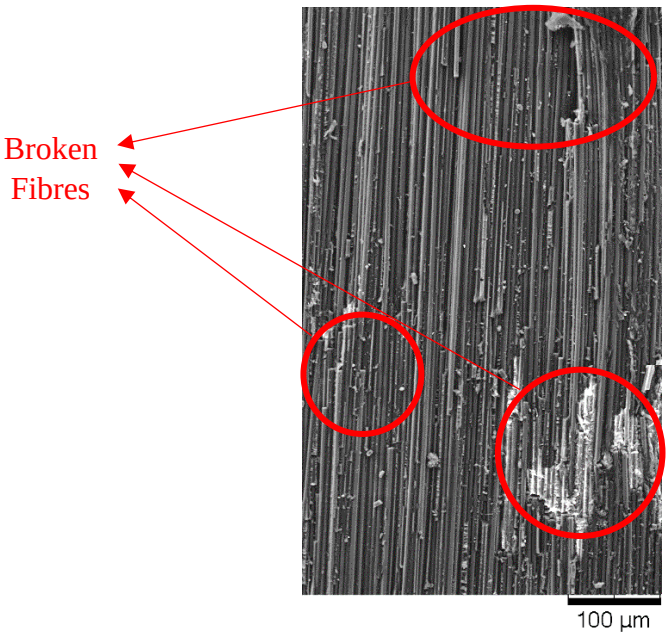

Figure 16 - Fracture surface of a DLJ after testing.

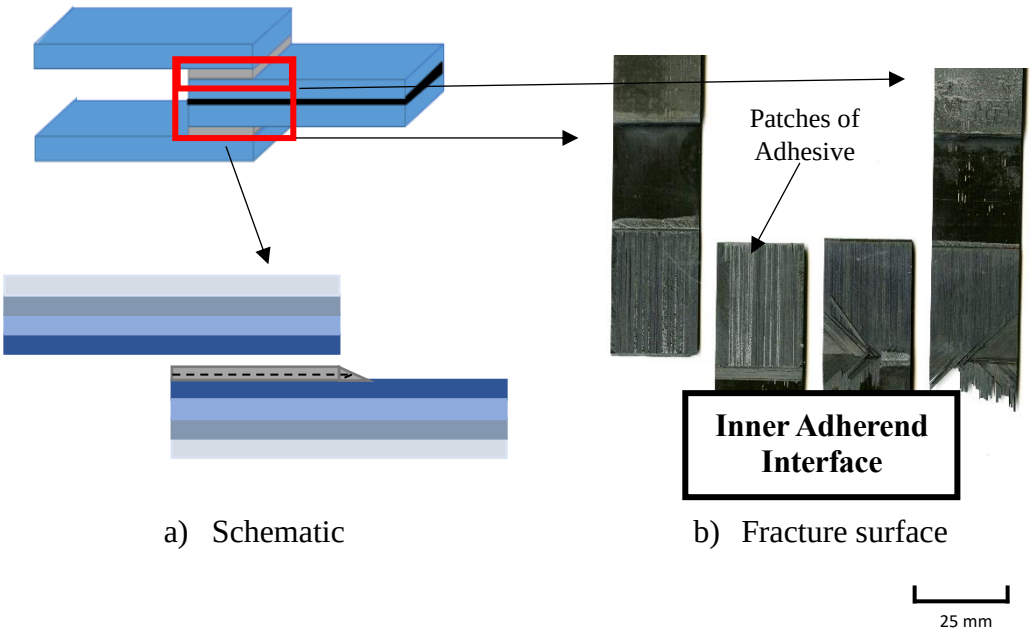

a) Schematic b) Fracture surface

Figure 17 - Failure schematic and fracture surface for plasma treated specimens.

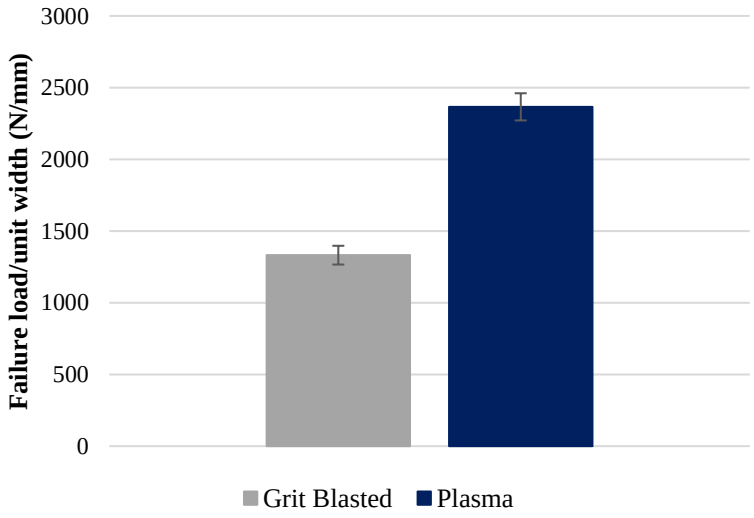

Figure 18 - Comparison of the plasma treated and grit blasted surface treatment for the DLJ strength.

Table 1 - Mode I test summary based on initial loading for the grit blasted and plasma treated specimens.

Adhesive Thickness	**Surface Preparation**	**Initiation- G_{IC} (N/mm) (CV)**	**Number of Specimens**
0.2 mm[a]	Grit Blasted	0.347 (16%)	3
	Plasma Treatment	0.864 (4%)	4
0.8 mm	Grit Blasted	1.211 (2%)	3
	Plasma Treatment	1.402 (3%)	3

[a] The results are based on Pmax.

Table 2 - Double Lap Joint strength for grit blasted and plasma treatment surface preparation.

Surface Treatment	**Failure load/unit width (N/mm) (CV)**	**Number of Specimens**
Grit Blasted	1332 (5%)	4
Plasma	2366 (4%)	4